DONALD D. DUNCAN, CHARLES H. LANGE, and DAVID G. FISCHER

IMAGING PERFORMANCE OF CRYSTALLINE AND POLYCRYSTALLINE OXIDES

Knowledge of the scatter characteristics of candidate infrared sensor dome materials is necessary for the evaluation of image quality and susceptibility to bright off-axis sources. For polycrystalline materials in particular, the scattering levels are high enough to warrant concern. To evaluate the effects of scatter on image quality, estimates of the window point spread function or its transform, the optical transfer function, are required. In addition, estimates of the material scatter cross section per unit volume are essential for determining flare susceptibility. Experimental procedures and models used at the Applied Physics Laboratory allow the determination of each. Measurement results are provided for samples of sapphire (ordinary ray), pure yttria, lanthanum-doped yttria, spinel, and ALON. Applications of these results are illustrated for planar windows having arbitrary orientations with respect to the optical axis.

INTRODUCTION

We will show that the total point spread function (PSF) is a weighted sum of one term due solely to diffraction and one that includes scatter effects. The latter term is given by the convolution of the PSF due to scatter and the PSF due to diffraction. For scatter, we demonstrate that the PSF is a linear mapping to the focal plane (in the paraxial approximation) of the scattering phase function. The weights on the two components of the total PSF are functions of the scatter cross section per unit volume. The PSF or its transform, the optical transfer function (OTF), provides a complete description of the imaging performance of the window.

Two experimental techniques are used: integrating sphere measurements for the total integrated scatter and forward-to-backscatter ratios, and direct measurement of the scattering phase function. Bulk measurements of the total integrated scatter are carried out using a three-wavelength (0.6328, 1.15, and 3.39 μm) HeNe laser. These data, combined with models for the first- and second-order scatter phenomena, yield estimates of bulk scatter cross section per unit volume. Direct measurements of the angular distribution of the scattered light at 0.6328 μm produce estimates of the phase function for scatter. By combining these two data sets, we can calculate the PSF for scatter, and thence its transform, the OTF.

THE OTF FOR SCATTER

Figure 1 shows a particular imaging configuration in which a point source at infinity is imaged by a lens system containing a scattering screen within the pupil. For this imaging configuration, Goodman[1] has shown that the total system OTF can be written as the product of the OTF due to diffraction and that due to the screen,

$$H_{\text{tot}}(\boldsymbol{\nu}) = H_{\text{diff}}(\boldsymbol{\nu}) H_{\text{screen}}(\boldsymbol{\nu}) , \qquad (1)$$

where $\boldsymbol{\nu}$ is a spatial frequency. The OTF for the screen, in turn, can be broken into a component due to unscattered light and one due to scattered light,

$$H_{\text{screen}}(\boldsymbol{\nu}) = \exp(-\beta_s L) + [1 - \exp(-\beta_s L)] H_{\text{scat}}(\boldsymbol{\nu}) , \qquad (2)$$

where β_s is the scatter cross section per unit volume, L is the physical thickness of the screen, and $H_{\text{scat}}(\boldsymbol{\nu})$ is the OTF for scatter. The components of this equation are shown in Figure 2A, wherein the dotted line is the asymptote to which the screen OTF falls for large spatial frequencies. This asymptote is due to the unscattered light. Equation 2 can be transformed to yield the PSF due to the screen,

$$h_{\text{screen}}(\mathbf{r}) = \exp(-\beta_s L)\,\delta(\mathbf{r}) + [1 - \exp(-\beta_s L)] h_{\text{scat}}(\mathbf{r}) , \qquad (3)$$

where $\mathbf{r}$ is the spatial coordinate and $\delta(\mathbf{r})$ is the Dirac delta function. The components of this equation are shown in Figure 2B. Here, the value of the asymptote to which the OTF falls for large spatial frequencies yields, under the Fourier transform, a delta function of area $\exp(-\beta_s L)$. The screen PSF appears as a bright spot (the delta function) surrounded by a diffuse halo caused by scatter.

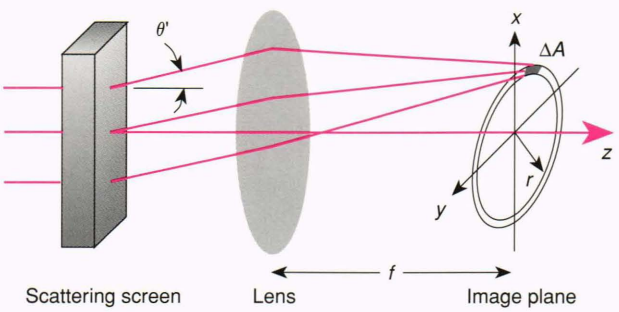

Figure 1. Configuration for calculating the point spread function of the scattering screen. For a scattering screen within the pupil of an imaging system, light scattered at polar angle θ' is brought to focus as an annulus within the image plane. (θ' = angle between the incident direction and the angle of scatter, f = focal length, r = radius, and ΔA = differential area.)

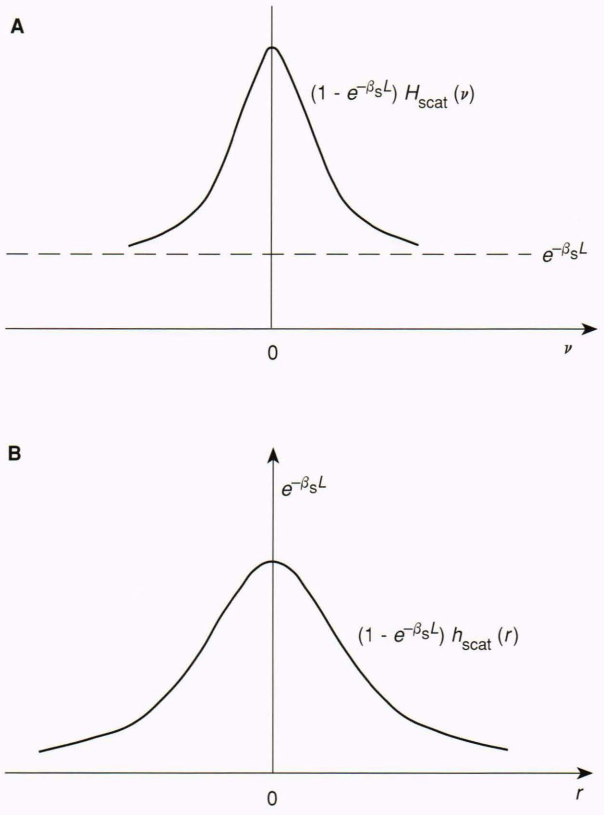

Figure 2. Illustration of effects due to scattering screen. **A.** Screen optical transfer function (OTF). The curve centered around zero spatial frequency represents the portion of the OTF due to scattered light; the asymptote to which this curve falls (dotted line) is due to unscattered light. **B.** Screen point spread function (PSF). The central delta function is due to unscattered light. The halo surrounding it is due to scattered light. (H_{scat} = portion of OTF due to scatter, h_{scat} = portion of PSF due to scatter, β_s = scatter cross section per unit volume, L = physical thickness of the screen, ν = spatial frequency, and r = radius.)

The resulting total system PSF is the convolution of the PSF's due to diffraction and the screen,

$$h_{tot}(\mathbf{r}) = \exp(-\beta_s L)\, h_{diff}(\mathbf{r}) + [1-\exp(-\beta_s L)] h_{scat}(\mathbf{r}) * h_{diff}(\mathbf{r}). \quad (4)$$

We can now derive the expression for the PSF due to scatter. Because a point source is being imaged, the output of the system will be, by definition, the system PSF. Without the screen present, a point source on axis at infinity will be imaged as a point on axis in the back focal plane of the lens; the PSF is simply that due to diffraction. With the screen present, however, the incoming light from the point source (a plane wave) will be redistributed according to the scattering phase function, $P(\theta)$, with the radiant intensity (power per unit solid angle) at angle θ given by

$$I_{scat}(\theta) = E_0 A_p [1-\exp(-\beta_s L)] P(\theta), \quad (5)$$

where E_0 is the incident intensity and A_p is the area of the pupil.[2] All light scattered at this angle will be focused by the lens into an annulus of differential width $r\Delta r$ (at radius r) in the back focal plane of the lens, where

$$r = f \tan\theta, \quad (6)$$

f is the focal length of the lens, and θ is the angle between the direction of the scattered light and the z axis. The incremental power falling on a differential area ΔA of the annulus is given by

$$\Delta\Phi(r) = E_0 A_p [1-\exp(-\beta_s L)] P(\theta) \frac{\Delta A}{f^2}, \quad (7)$$

where $\Delta A/f^2$ is the solid angle subtended by the area ΔA. The intensity in the back focal plane at a distance r off axis is therefore given by

$$E(r) = E_0 A_p [1-\exp(-\beta_s L)]\, P[\tan^{-1}(r/f)] \frac{1}{f^2}. \quad (8)$$

The PSF for scatter is then simply an amplitude-scaled version of this intensity such that the volume under the PSF (the integral over the focal plane) is unity. This result is rather interesting. The phase function can be viewed as the probability density function (PDF) of the scatter angle (i.e., the ray slopes). (An identical result is seen with strong turbulence.[1]) The PSF then is merely a mapping of this PDF to the system focal plane. This simple conceptual result for an idealized geometry (normal incidence on a flat scattering screen) makes the generalization to more complicated geometries extremely easy.

The preceding is a simplified version of what actually happens. We have ignored the refraction that occurs at the window/air interface. Because of this effect, the scatter angle external to the screen is altered with respect to the angle within the screen in accord with Snell's law. In addition, the solid angle into which the light is scattered is increased. Each of these effects was accounted for in the measurement of the bulk phase functions, which is described next. When we deal with applications of these results later in this article, we also consider these effects.

MODELS AND MEASUREMENT PROCEDURES

In what follows, we discuss the models and procedures used to determine the scatter cross sections per unit volume and the scatter phase functions. The actual results of these measurements are detailed in a subsequent section.

Scatter Cross Sections

Figure 3 schematically shows the scattering measurement. The output from a three-color HeNe laser was chopped and directed into a 6-in.-dia. integrating sphere. The detector was mounted on the wall of the sphere and produced a signal proportional to the radiation collected by the sphere. Detector output was monitored by a lock-in amplifier. For measurements in the visible, a large-area silicon detector was used. Measurements in the near- and mid-IR were made with a pyroelectric detector.

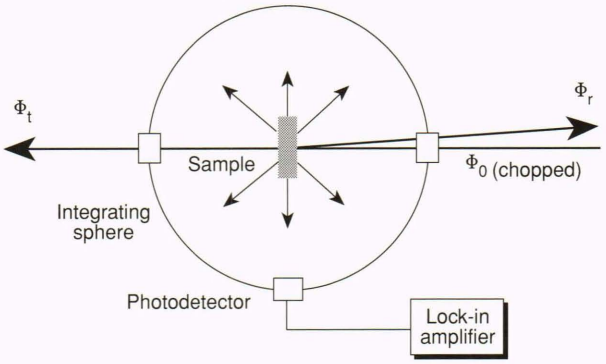

Figure 3. Integrating sphere measurement of the scattered power Φ_s. The incident, reflected, and transmitted power are denoted Φ_0, Φ_r, and Φ_t, respectively. The incident light is modulated by a chopper, and the detection is performed synchronously with this modulation.

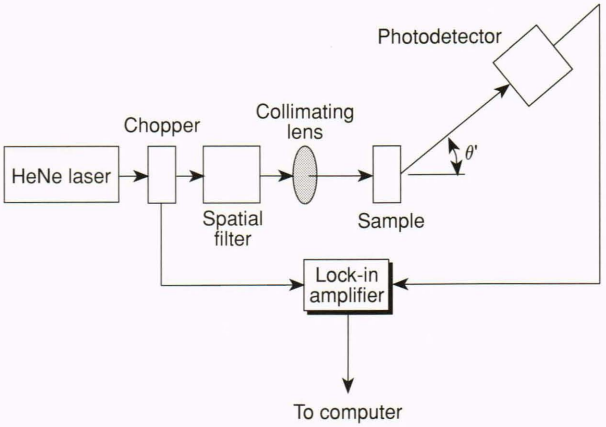

Figure 4. Phase function measurement configuration. The photodetector is swung through an angle θ' that ranges from 0.5° to 45°.

Before measuring scatter, we established the integrating sphere calibration factor F (ratio of the power introduced into the sphere and the power measured at the sphere's surface). Then, to determine the scatter cross section per unit volume within the visible (where absorption was assumed negligible), we performed two separate measurements for each sample: one was of the incident power, Φ_0, and the other was the measurement with the sample mounted within the sphere, Φ_s. In the latter, the beam transmitted by the sample (unscattered portion of the incident beam) was allowed to escape through the exit port of the sphere. The relationship between these quantities is then

$$\Phi_s = \frac{\Phi_0}{F}(1-R)\left(1+R-R\beta_s L\right)\beta_s L\,, \tag{9}$$

where R is the Fresnel (power) reflection coefficient and we have assumed that $\beta_s L << 1$.

The measurement technique in the visible was based on the assumption that extinction was due strictly to scatter. For measurements in the near- and mid-IR, this assumption (of negligible absorption) is not justified.[3] Therefore, a third measurement was required, in which the transmitted beam was also constrained to remain within the sphere by placing a conical scatter target within the exit port.

Bulk Phase Functions

Figure 4 shows the apparatus with which scatter phase functions were measured. The beam from a randomly polarized 5-mW HeNe laser was chopped and spatially filtered, then collimated and passed through the sample. Scattered light was measured using a silicon photodetector mounted on a rail, which was, in turn, mounted on a rotational stage. The rotational stage allowed us to measure the scattered light as a function of angle, and the rail allowed us to adjust the distance from the detector to the sample. The output of the detector (proportional to scattered power) was monitored by a lock-in amplifier, whose reference signal was derived from the chopper.

The scattered radiant intensity is distributed with angle according to

$$I_s(\theta) = \Phi_0 \beta_s L P(\theta)\,, \tag{10}$$

where $I_s(\theta)$ is the scattered power per unit solid angle, $P(\theta)$ is the phase function, and θ is an angle measured from the direction of incidence and within the scatter plane. Actually, $P(\theta)$ is the arithmetic average of $P_1(\theta)$ and $P_2(\theta)$, which are the phase functions for polarization perpendicular to and within the plane of scatter, respectively.[2] By defining $P(\theta)$ in this manner, we implicitly assume that the incident radiation is unpolarized. In addition, the scatter is assumed to be symmetric with respect to the direction of incidence; that is, the scatter has no angular dependence in the plane normal to the direction of incidence. Consequently, the scattered power at angle θ falling on an area subtending a solid angle Ω_θ is given by

$$\Phi_s(\theta) = \Phi_0 \beta_s L P(\theta) \Omega_\theta\,. \tag{11}$$

The inverse of this equation yields the following expression for the phase function:

$$P(\theta) = \frac{1}{c}\frac{\Phi_s(\theta)}{\Omega_\theta}\,, \tag{12}$$

where those quantities independent of θ have been lumped into the constant c. The constant is defined such that the integral of the phase function over 4π steradians is unity. This normalization of $P(\theta)$ emphasizes its interpretation as a PDF for the scatter direction.

The expression given in Equation 11 for the scattered intensity is defined in terms of quantities that are measured inside the dielectric screen. In a practical situation, however, the quantities of interest, namely, the scattered power observed at the detector and the solid angle subtended by the detector, are measured some distance outside the screen. Therefore, one must relate those quantities in the defining equation for $P(\theta)$ to those that

are actually measured. First, a relationship must be established between the scattered powers inside and outside the screen. Assuming unpolarized light incident on the screen, the scattered power at angle θ inside the screen is given by

$$\Phi_s(\theta) = \frac{2}{(T_{\|} + T_{\perp})} \Phi_s(\theta'), \qquad (13)$$

where $T_{\|}$ and $T_{\perp}$ are the Fresnel transmission formulae, and $\Phi_s(\theta')$ is the scattered power measured at the detector for an angle θ' with respect to the interface normal (Fig. 5). Next, the solid angle Ω_θ subtended in the screen at angle θ must be expressed in terms of quantities outside the screen, namely, the angle θ' between the detector and the interface normal and the distance R from the screen to the detector. With reference to Figure 5, this solid angle is given approximately by

$$\Omega_\theta \approx \frac{\pi}{n} (\alpha/2)^2 \frac{\cos\theta'}{\left(n^2 - \sin^2\theta'\right)^{1/2}}, \qquad (14)$$

where n is the refractive index and α is the full linear angle subtended at the scattering volume by the detector ($\alpha \approx r/R$). The phase function $P(\theta)$ is therefore defined in terms of measurable quantities, and once the constant c is determined by the normalization condition, it is uniquely specified.

RESULTS

Results of the measurements of bulk scatter per unit length, b_s, are summarized in Tables 1 through 3 for wavelengths of 0.6328, 1.15, and 3.39 mm, respectively. Included in Table 1 is the variation in scatter, $(b_{max}\ 2\ b_{min})/(b_{max} + b_{min})$, across the sample. In each situation, the estimated measurement uncertainty in the scatter was less than the variation across the sample.

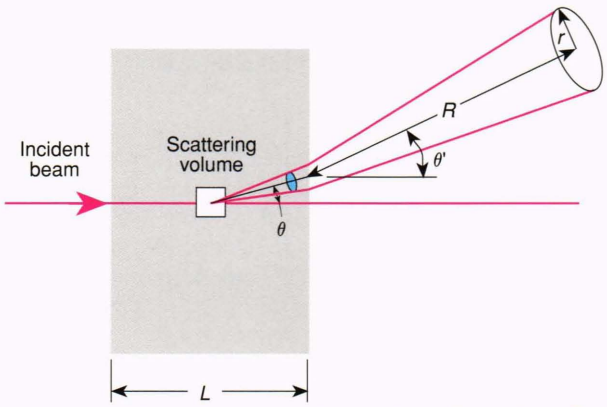

Figure 5. Solid angle relationship at a dielectric interface. Because of refraction at the interface, the solid angle subtended by a circular detector of radius r outside the scattering screen is mapped to a solid angle with an elliptical cross section within the screen. The shaded area (blue) is the elliptical cross section subtending a solid angle Ω. (R = distance to detector, L = physical thickness of the screen, and θ and θ' are related through Snell's law for refraction at the interface.)

Tables 1 and 2 show measured values of forward-to-backscatter ratios, F_f/F_b. The substantial values of these ratios are indicative of scatterers that are very large with respect to the wavelength. Sapphire displayed very low scatter levels in the visible and unmeasurable levels in the near- and mid-IR. Figure 6 shows the wavelength-dependence of the scatter cross section per unit volume. Similar results were obtained for each material for which measurements could be made at all three wavelengths. This wavelength-dependence is summarized in Table 4.

Apparent phase function measurements were made at 0.6328 μm. Samples were placed in the apparatus shown in Figure 4, and measurements were made for angles between 0.5° and 45°. In deriving the bulk scatter phase function from the measured data, the Fresnel reflections and modification of the solid angles due to refraction at

Table 1. Scattering results at 0.6328 μm.

Sample	Thickness (cm)	β_s (cm^{-1})	Variation	Φ_f/Φ_b
Spinel				
26	0.318	0.297	0.204	3.13
30	0.310	0.317	0.027	3.60
31	0.310	0.271	0.027	3.45
32	0.310	0.279	0.022	2.91
41	0.630	0.713	0.007	6.31
42	0.630	0.842	0.007	6.25
Sapphire				
1	0.318	0.007	0.116	1.82
2	0.318	0.007	0.262	2.43
62	0.318	0.011	0.160	2.40
65	0.102	0.034	0.123	2.65
66	0.102	0.027	0.086	2.38
ccs3	0.102	0.030	0.153	2.00
ALON				
A1	0.104	0.444	0.043	7.58
A2	0.104	0.154	0.108	6.10
B1	0.635	0.476	0.046	10.6
B2	0.635	0.152	0.021	8.41
Yttria (pure)				
5	0.102	1.273	0.065	4.81
16	0.635	0.732	0.039	7.38
47	0.211	0.941	0.030	5.09
48	0.211	0.872	0.014	4.37
49	0.607	0.717	0.011	6.71
50	0.605	0.741	0.008	5.71
Yttria (lanthanum-doped)				
21	0.102	1.174	0.068	2.97
22	0.554	0.726	0.109	3.88
23	0.592	0.415	0.039	4.89
24	0.594	0.346	0.082	4.56
25	0.198	0.623	0.192	4.55
26	0.196	0.412	0.016	4.53
27	0.257	1.195	0.051	5.08

Note: β_s = bulk scatter per unit length. Φ_f/Φ_b = forward-to-backscatter ratio.

Table 2. Scattering results at 1.15 μm.

Sample	β_s (cm^{-1})	Φ_f/Φ_b
Spinel		
26	0.129	1.73
30	0.138	2.54
41	0.342	3.43
ALON		
A1	0.384	2.43
B1	0.261	4.37
Yttria (pure)		
5	0.348	1.74
47	0.254	1.49
49	0.272	2.70
Yttria (lanthanum-doped)		
21	0.514	1.45
24	0.153	2.16
26	0.249	2.03
27	0.633	1.91

Note: β_s = bulk scatter per unit length. Φ_f/Φ_b = forward-to-backscatter ratio.

Table 3. Scattering results at 3.39 μm.

Sample	β_s (cm^{-1})
Spinel	
26	0.046
30	0.032
41	0.051
ALON	
A1	0.107
B1	0.073
Yttria (pure)	
5	0.082
47	0.033
49	0.032
Yttria (lanthanum-doped)	
21	0.117
24	0.061
26	0.135
27	0.250

Note: β_s = bulk scatter per unit length.

the sample interface were accounted for. Bulk scatter phase functions generally were strongly peaked in the forward direction. For ALON, however (Fig. 7), the maximum measured value of the phase function occurred at about 0.72°; this behavior manifests itself as a distinct halo in the focal plane. The existence of a halo suggests that the scatterers are of uniform size. In the geometrical optics regime, scatter from a circular opaque disc produces an Airy distribution[4] with a secondary peak at an off-axis angle of 1.635 λ/D, where λ is the wavelength of the incident light, and D is the diameter of the disc. Likening the scatterers to opaque discs produced a diameter estimate of 82 μm.

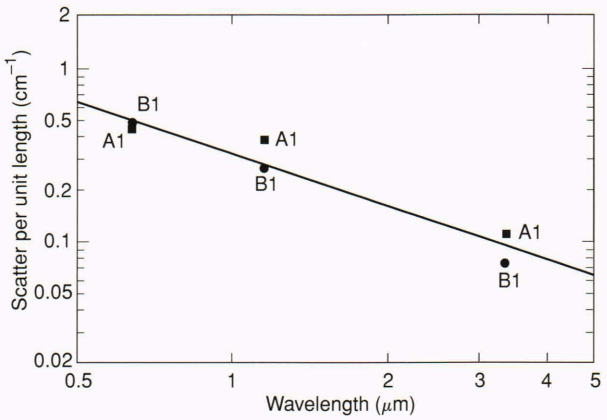

Figure 6. Wavelength-dependence of scatter cross sections per unit volume for ALON (samples A1 and B1).

Table 4. Wavelength-dependence of scatter.

Material	β_0 (cm^{-1})	γ	No. of samples	Correlation coefficient
Spinel	0.220	1.35	9	0.93
ALON	0.317	1.01	6	0.97
Yttria (pure)	0.397	1.82	9	0.97
Yttria (lanthanum-doped)	0.408	0.99	12	0.78

Note: $\beta_s = \beta_0 \lambda^{-\gamma}$ is the model fit to the data by least squares. β_0 and γ are the resulting parameter estimates (λ in μm).

One oft-quoted figure of merit of imaging quality is the modulation transfer function (MTF), which is simply the modulus of the OTF. Examples of representative MTF's for scatter are shown in Figure 8. The cusp in the curve for ALON near 28 cycles/rad indicates a contrast reversal.

APPLICATIONS

For a scattering screen at an arbitrary orientation (Fig. 9), we can formulate the PSF in terms of the angular separation between the nominal ray direction, $\hat{a}$, and an arbitrary ray direction, $\hat{b}$. These ray directions are related to the ray directions inside the scatter screen via Snell's law,

$$\begin{aligned} n\hat{e}\times\hat{\alpha} &= \hat{e}\times\hat{a} \\ n\hat{e}\times\hat{\beta} &= \hat{e}\times\hat{b}\,, \end{aligned} \tag{15}$$

where $\hat{e}$ and n are the screen normal and its refractive index, respectively. Because the ray positions are continuous across a dielectric interface, the unit vectors $\hat{\alpha}$ and $\hat{a}$, for example, lie within a plane. Within this plane, Snell's law takes on the more familiar form:

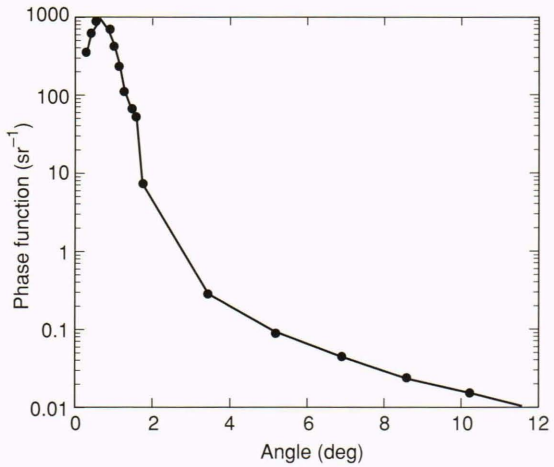

Figure 7. Phase function for ALON (sample B2).

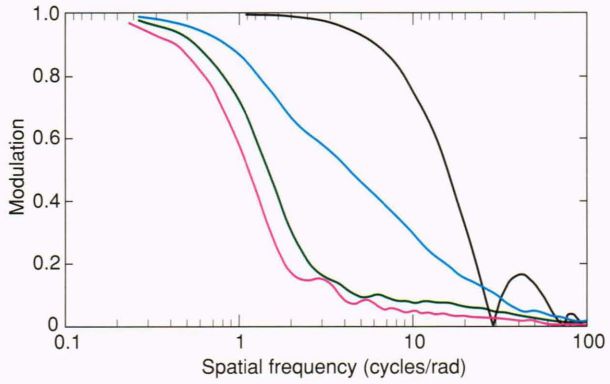

Figure 8. Typical modulation transfer functions of spinel sample 41 (red curve), pure yttria sample 5 (green curve), lanthanum-doped yttria sample 24 (blue curve), and ALON sample B2 (black curve).

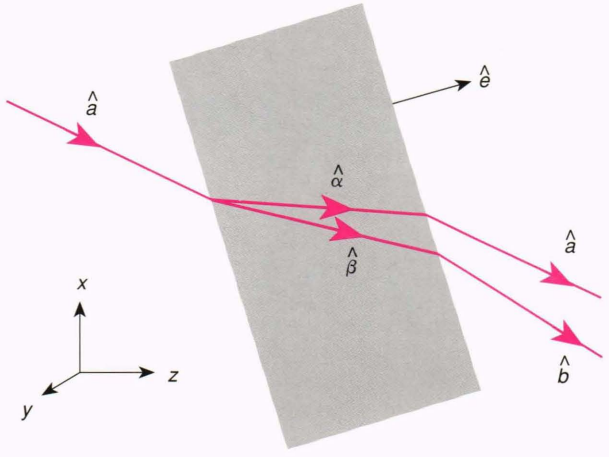

Figure 9. Tilted plate geometry. Unit vectors $\hat{a}\,(\hat{\alpha})$ and $\hat{b}\,(\hat{\beta})$ represent, respectively, the incident and scattered ray directions outside (inside) the scattering screen whose orientation is denoted by its unit normal, $\hat{e}$.

$$n\sin(\hat{e},\hat{a}) = \sin(\hat{e},\hat{a})\,. \tag{16}$$

Now the PSF for scatter is given simply by

$$PSF \propto P[\cos^{-1}(\hat{\alpha}\cdot\hat{\beta})]\,. \tag{17}$$

The unit vectors $\hat{\alpha}$ and $\hat{\beta}$ can be solved for by forming the vector cross product of $\hat{e}$ from the left with Equation 15 and using the vector identity

$$\mathbf{A}\times\mathbf{B}\times\mathbf{C} = \mathbf{B}(\mathbf{AC}) - \mathbf{C}(\mathbf{AB})\,. \tag{18}$$

The result is

$$\hat{\alpha}\cdot\hat{\beta} = (1/n^2)[(\hat{a}\cdot\hat{b}) - (\hat{e}\cdot\hat{a})(\hat{e}\cdot\hat{b}) + (n^2 - |\hat{e}\times\hat{a}|^2)^{1/2}(n^2 - |\hat{e}\times\hat{b}|^2)^{1/2}], \tag{19}$$

where we have also used the relationship

$$n\cos(\hat{e},\hat{\alpha}) = [n^2 - \sin^2(\hat{e},\hat{\alpha})]^{1/2}\,. \tag{20}$$

These results are shown in Figure 10 by the gray-level representations of the PSF's for ALON sample B2. The region shown in the figure is 0.125×0.125 radian in the focal plane. Results for Figures 10A and 10B are $\hat{e}$ = (0, 0, 1) and $\hat{e}$ = (−0.50, −0.50, 0.707), respectively. The vertical line through the center of the figure represents the position at which the PSF profile is taken (the curve whose baseline is along the left vertical axis). As seen in Figure 10B, the effect of a tilt in the scattering screen is to broaden the PSF and to stretch it along the projection onto the focal plane of the tilt vector. Similar results are shown in Figure 11 for yttria sample 5.

This formalism can be extrapolated easily to other wavelengths. Recall that the phase functions are highly peaked in the forward direction. Furthermore, at least for ALON and doped yttria, little wavelength-dependence for scatter (Table 4) is seen. These results suggest that the scatterers are large with respect to the wavelength; that is, we are in the geometrical optics regime in which the angular scatter pattern is approximately λ/D (full width at half maximum), where D is the diameter of the scatterer. By measuring the phase function width at one wavelength, we therefore can infer the width at another wavelength, subject only to the restriction that the dimension of the scatterer is large compared with the wavelength.

CONCLUSION

Scatter properties directly affect the imaging characteristics of the candidate window materials. The greater the sample scatter, the stronger the diffuse portion of the PSF compared with its large, on-axis, unscattered component. In the geometrical optics regime, the width of the phase function (and thus the PSF) is directly proportional to the wavelength-to-scatterer size ratio. At IR wavelengths, it follows that the PSF's will be wider than at 0.6328 μm; however, the scattering coefficients are generally smaller (Table 4), and image degradation due to the wider PSF will be less pronounced.

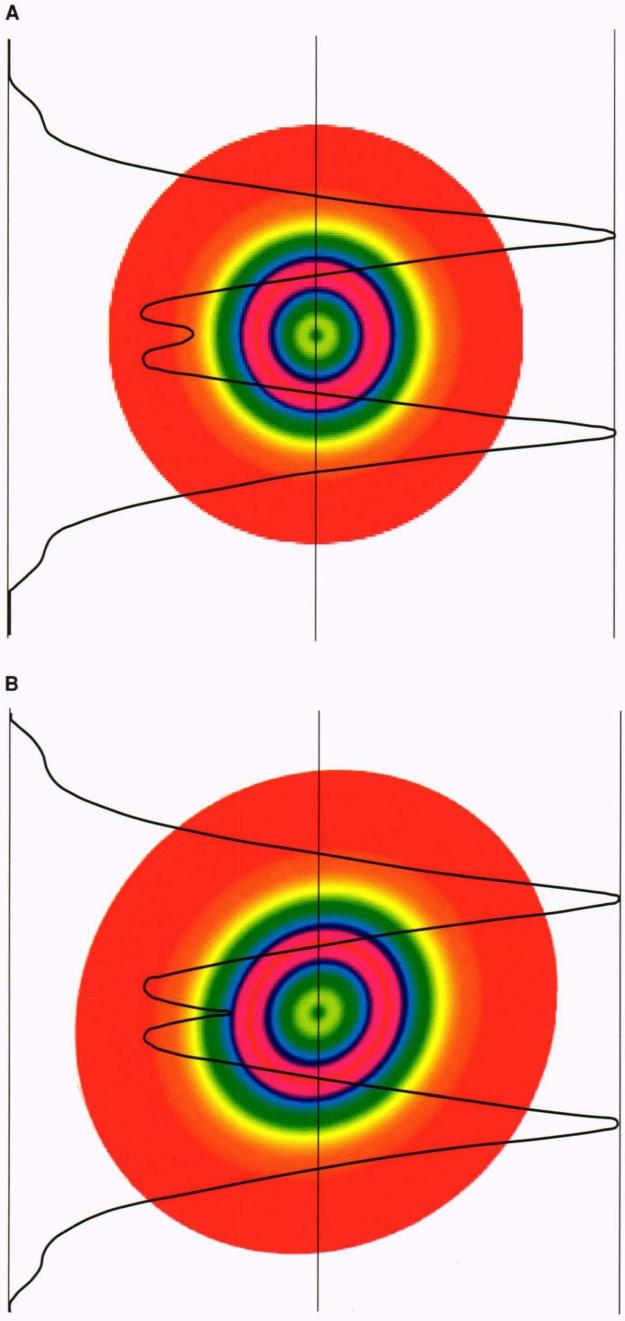

Figure 10. Point spread function for ALON sample B2. **A.** Scatter screen normal ($\hat{e}$) to optical axis, $\hat{e}$ = (0, 0, 1). **B.** Tilted scatter screen, $\hat{e}$ = (−0.50, −0.50, 0.707).

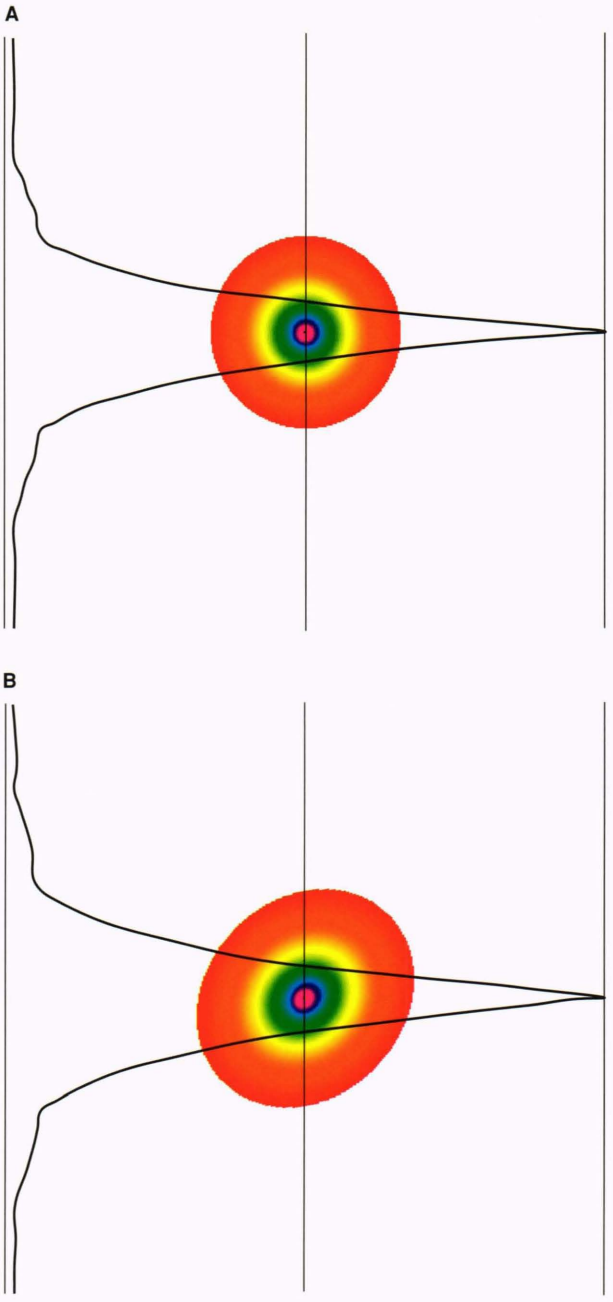

Figure 11. Point spread function for yttria sample 5. **A.** Scatter screen normal ($\hat{e}$) to optical axis, $\hat{e}$ = (0, 0, 1). **B.** Tilted scatter screen, $\hat{e}$ = (−0.5, −0.5, 0.707).

REFERENCES

[1] Goodman, J. W., *Statistical Optics*, John Wiley & Sons, New York (1985).
[2] Deirmendjian, D., *Electromagnetic Scattering on Spherical Polydispersions*, American Elsevier Publishing Co., New York (1969).
[3] Thomas, M. E., and Joseph, R. I., "A Comprehensive Model for the Intrinsic Transmission Properties of Optical Materials," in *Proc. SPIE on Infrared Optical Materials VI*, Vol. 929, pp. 87-93 (Apr 1988).
[4] Born, M., and Wolf, E., *Principles of Optics*, 4th Ed., Pergamon Press, Oxford (1970).

THE AUTHORS

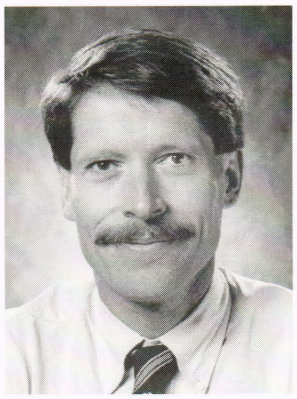

DONALD D. DUNCAN is supervisor of the Measurements and Propagation Section of APL's Electro-Optical Systems Group. He received his Ph.D. in electrical engineering from The Ohio State University in 1977. From 1977 to 1983, he was employed by Pacific-Sierra Research Corporation, where he modeled optical propagation phenomena such as aerosol scatter, atmospheric turbulence, and high-energy laser effects (e.g. thermal blooming, aerosol burn-off). Since joining APL in 1983, Dr. Duncan has worked on various biomedical engineering projects; provided test program support and data analysis for a tracking/guidance synthetic aperture radar system; and worked on many measurement, modeling, and diagnostic equipment projects in support of the hypersonic interceptor. He also teaches courses in Fourier and statistical optics at The Johns Hopkins University G.W.C. Whiting School of Engineering.

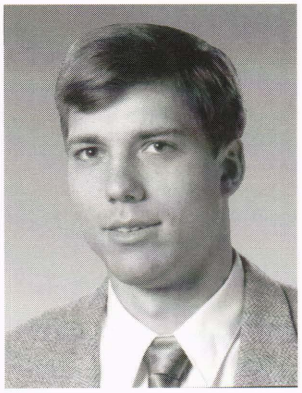

CHARLES H. LANGE is a member of APL's Associate Staff. He received his M.S. in electrical engineering from Texas A&M University in 1989, where his thesis work involved measurement, using optical modulation, of the intrinsic frequency response of semiconductor lasers. Since joining APL, he has worked on the characterization of polycrystalline materials, including bulk scatter properties and the dependence of refractive index on temperature. He has been involved with the alignment and characterization of an IR missile test facility whose purpose is to evaluate the dynamic tracking characteristics of missile seekers. Mr. Lange is currently the principal investigator on an independent research and development project aimed at developing infrared spatial light modulators using vanadium dioxide, and he also is the lead engineer for a set of space-borne imaging spectrographs.

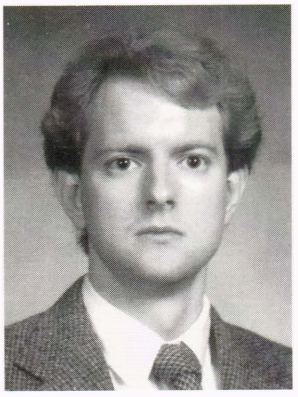

DAVID G. FISCHER received B.S. and M.S. degrees in electrical engineering from The Johns Hopkins University in 1988 and 1989, respectively. During 1988 and 1989, he was employed at APL as an associate research staff member. His work at the Laboratory involved modeling the scatter and imaging characteristics of polycrystalline dome materials. Since 1989 he has been at the Institute of Optics, University of Rochester, where he is a Ph.D. candidate in optics. His thesis research involves the theory of direct and inverse scattering from random media. Mr. Fischer is a member of Eta Kappa Nu, the Institute of Electrical and Electronics Engineers, and the Optical Society of America.